Colloids and Surfaces, 52 (1991) 9–34
Elsevier Science Publishers B.V., Amsterdam

Forces between solid surfaces in binary solutions

T.K. Vanderlick*, L.E. Scriven and H.T. Davis

University of Minnesota, Department of Chemical Engineering and Materials Science, 421 Washington Avenue S.E., Minneapolis, MN 55455 (U.S.A.)

(Received 28 November 1989; accepted 18 January 1990)

Abstract

Experimental measurements of the solvation forces between mica surfaces immersed in a binary solution of octamethylcyclotetrasiloxane and cyclohexane are reported. At all bulk concentrations examined (0–14, 32 and 42 mol% cyclohexane), the force varies between attraction and repulsion as the surface separation is decreased. The magnitudes of the forces at the attractive force minima decay exponentially with surface separation. The characteristic decay length and the average separation between attractive minima are functions of the bulk concentration. The statistical mechanics of inhomogeneous one-dimensional hard rod mixtures can be used to interpret the experimental results. The distribution functions and thermodynamic properties of a multicomponent hard rod fluid confined in a one-dimensional slit-pore are summarized. Density profiles and disjoining pressures are calculated as functions of pore width. Because of mechanical instabilities associated with the force measurement technique as presently used, not all theoretically predicted force minima (and maxima) are experimentally accessible.

1. INTRODUCTION

The behavior of liquids confined by solid surfaces to microscopic dimensions in at least one or more directions is of great interest to scientists and engineers seeking to understand the basic mechanisms of colloidal interactions, wetting and spreading, lubrication, membrane separations, sol-gel fabrication, and the like. Solid surfaces induce microstructure in liquids. The molecular structuring of liquid between solid surfaces gives rise to an anisotropic state of stress in the liquid that depends on the clearance between the surfaces. Hence, at most separations, confinement of a liquid requires exerting on the walls a normal stress different from the pressure in bulk liquid at the same temperature and pressure.

In the late seventies, van Megen and Snook [1] used the Monte Carlo method of computer simulation to model the behavior of liquid confined between smooth

*Present address: University of Pennsylvania, Department of Chemical Engineering, Philadelphia, PA 19104-6393, U.S.A.

0166-6622/91/$03.50

planar parallel solid surfaces separated by distances of a few molecular diameters. They discovered that as the separation of the walls diminished, the force on them, which they termed the "solvation force", oscillated with increasing amplitude between repulsion and attraction. Similar results were also predicted by Lane and Spurling [2]. These theoretical findings were corroborated by the pioneering work of Horn and Israelachvili [3,4] who used the surface forces apparatus to measure directly the solvation force on curved mica surfaces immersed in the silicone oil octamethylcyclotetrasiloxane (OMCTS), $[(CH_3)_2SiO]_4$.

Characteristics of the solvation force in pure liquids between solids are now well established. The strength and range of the force, which increases with decreasing separation between the solids, are influenced by the size, shape, and flexibility of the liquid molecules. In liquids whose molecules are nearly spherical, such as OMCTS, cyclohexane and tetrachloromethane, there are as many as ten measurable oscillations of the force between attraction and repulsion [5]. The period of the oscillations is approximately equal to the diameter of the liquid molecules. In linear alkanes, whose molecules are long and flexible, there are fewer measurable oscillations of the force, generally not more than four, the period being approximately equal to the width of the alkane chains [6].

The last decade has seen major advances in the development of molecular theories of inhomogeneous fluid, such as the generalized van der Waals theory of Nordholm and coworkers [7,8], the free energy density functional theory of Tarazona [9], of Meister and Kroll [10], and of Curtin and Ashcroft [11], the generalized hard rod theory, proposed independently by Robledo and Varea [12] and by Fischer and Heinbuch [13], and the Yvon–Born–Green distribution function theory with the Fischer–Methfessel closure approximation [14]. All have been relatively successful at qualitatively predicting the molecular structuring of a single-component fluid induced by excluded volume effects. One problem has been identified with the generalized van der Waals theory; namely, when applied to a van der Waals fluid at sufficiently high chemical potentials it admits solutions with negative densities [15]. The molecular theories just named, excepting those of Meister and Kroll [10] and Curtin and Ashcroft [11], were recently compared as they apply to a single-component fluid confined between solid surfaces [16].

Comparatively little effort has been directed to measuring, predicting and understanding the forces required to confine multicomponent fluids between solid surfaces. Christenson and Blom [17] examined systematically the effect of water in nonpolar liquids confined between mica surfaces; their study was largely motivated by previous observations [4,18] that solvation forces in nonpolar liquids are sensitive to trace amounts of dissolved water. Previously, Christenson [19] measured solvation forces in mixtures of two miscible non-

polar liquids (OMCTS and cyclohexane) confined between mica surfaces; however, he investigated only a few different bulk liquid concentrations.

On the theoretical front, little effort has been made to extend systematically molecular theories of an inhomogeneous fluid to multicomponent fluids. Two notable exceptions are the multicomponent extensions of the generalized van der Waals theory [20] and the YBG distribution function theory [21]. The multicomponent generalized van der Waals theory is, however, unsatisfactory for two reasons: the inadequacy of the single-component version of the theory that is manifested at high density, and the absence of an accurate equation of state of multicomponent fluid as underpinning. The YBG theory is based on mechanical equilibrium, and so cannot be applied to open systems in which the chemical potentials are the controlled field variables.

One benchmark in testing and guide in developing approximate theories of an inhomogeneous fluid is the exact theory of one-dimensional hard rods in an external field. The statistical mechanics of this system can be solved for exactly. In 1976, Percus [22] developed the distribution functions of hard rods in an arbitrary external field, and recently this was extended to multicomponent systems [23].

This paper has two main parts. In Section 2, we report our measurements of the solvation forces in binary solutions of OMCTS and cyclohexane confined between mica surfaces; these measurements constitute a more thorough and systematic continuation of the measurements of Christenson [19] on the same system. In Section 3, we consider the theory of open isothermal systems of one-dimensional hard rod mixtures confined in a slit-pore, i.e., on a line of finite length, and present analytical expressions for the equilibrium properties of this system; in Section 4, we use these to understand and interpret the experimental results.

2. SURFACE FORCES EXPERIMENTS

The experimental section is divided into four parts. In Section 2.1, we describe the design and operation of the surface forces apparatus with particular attention devoted to the role of mechanical instabilities in measuring force curves. An understanding of such instabilities is critical to relating the experimental results with the theoretical predictions for the binary hard rod system. In Section 2.2, we summarize the experimental method. In Section 2.3 we report our measurements of the solvation forces in pure OMCTS and pure cyclohexane between mica surfaces; our results are compared with those obtained by Christenson and coworkers [5,17]. Furthermore, for the first time, a statistical analysis is brought to bear in interpreting the experimental findings. In Section 2.4 we report measurements of the solvation forces in mixtures of OMCTS and cyclohexane between mica surfaces.

2.1. Description of the surface forces apparatus

The force required to confine a liquid film between two solid surfaces can be directly measured with the surface forces apparatus. With this apparatus, one can measure the distance between two molecularly smooth mica sheets with a precision of ± 1 Å and the forces on these surfaces with a sensitivity of millidynes. The surface separation can be varied over a range of microns, in increments as small as ångstroms.

The surface forces apparatus was designed in Tabor's laboratory at Cambridge University in the late 1960's [24] and refined into the form used here by Israelachvili and Adams [25]. A schematic of the apparatus is shown in Fig. 1. The mica sheets are glued onto cylindrical lenses of quartz whose axes are oriented perpendicular to one another. The upper lens is mounted on a fixed support whereas the lower lens is mounted at the end of a leaf spring of known spring constant.

In the experiment, the deflection of the leaf spring supporting the lower surface is measured as a function of the separation between the mica sheets. The force required to confine the liquid between the mica surfaces is, by Hooke's

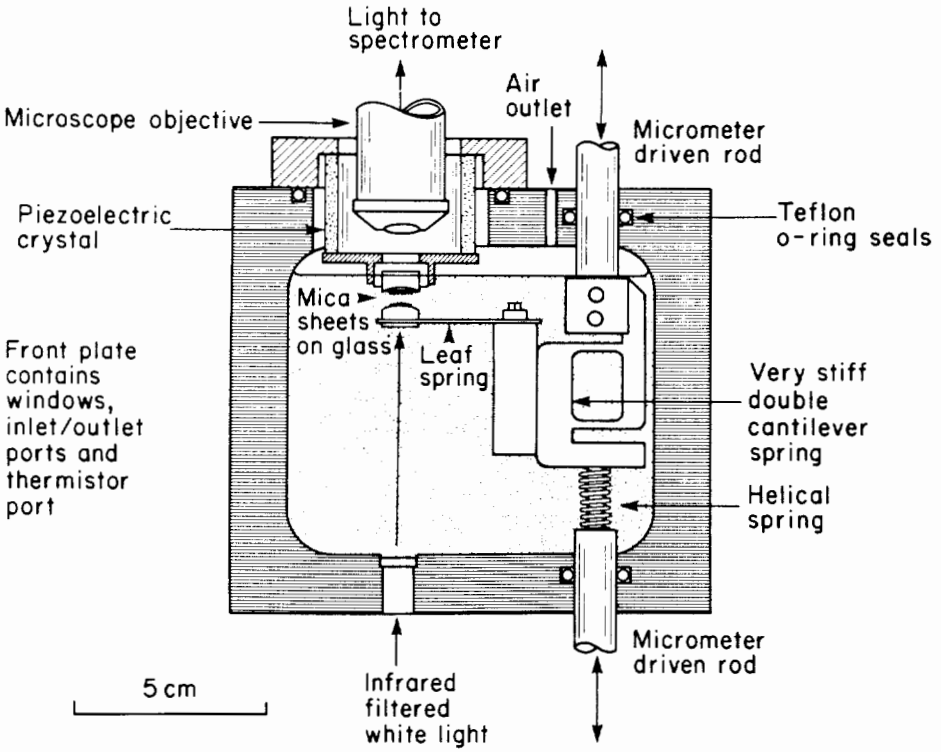

Fig. 1. Schematic of the surface forces apparatus.

law, proportional to the deflection of the spring. It is useful to distinguish between two separations. The *surface separation* is the distance between the mica surfaces. The *reference separation* is the distance between the top mica surface and the base of the leaf spring. The spring deflection is then equal to the difference between the surface separation and the reference separation.

The reference separation can be changed by one of three methods. The base of the leaf spring can be mechanically moved coarsely (microns) by the upper motor-driven micrometer screw, or finely (nanometers) by the lower motor-driven micrometer screw. The lower screw operates on a differential spring mechanism consisting of a weak helical spring in tandem with a stiff double cantilever spring, the latter being roughly one thousand times stiffer than the former. A displacement of the lower micrometer screw thus induces a displacement of the base of the leaf spring that is reduced by a factor of one thousand. The synchronous motor which drives the lower micrometer screw is coupled to a variable resistance potentiometer, thus allowing resistance to be recorded as the screw is turned. The ability to change mechanically the reference separation by nanometers, over a range of microns, is the forte of the apparatus. Changes in reference separation down to ångstroms can be obtained by mounting the upper surface on a piezoelectric crystal tube which expands or contracts in response to an applied voltage.

The surface separation is measured by multiple beam interferometry. Before the mica sheets are glued onto the quartz lenses, a thin film of silver (ca 560 Å) is deposited on the side of the mica sheet which will contact the glue. The resulting silver–mica–medium–mica–silver sandwich constitutes an interferometer. When white light is passed through it, only discrete wavelengths interfere constructively and are transmitted. The transmitted light is focused onto the slit of a spectrometer, where it is dispersed into its component wavelengths and can be viewed as a series of fringes. The wavelengths of the fringes vary continuously with surface separation and can be used to determine the separation relative to a reference state, which is usually the closest approach of the mica surfaces in air.

The apparatus is used to measure forces in the following way. First the methods used to change the reference separation are calibrated. This is done at surface separation large enough that no force is present and so the spring is not deflected. Hence, the induced change in reference separation, as monitored by the resistance (lower micrometer screw) or applied voltage (piezoelectric crystal), is equal to the change in surface separation, which is measured optically. This is illustrated in Fig. 2A. The calibration constant, $dD/d\alpha$, representing the change in reference separation per unit α is thus determined, where α is either resistance or voltage, depending on the mechanism used to change the reference separation. Thereafter, the reference separation is changed by calibrated amounts and the resulting change in separation between the surfaces is measured. This is illustrated in Fig. 2B. Consequently, the difference

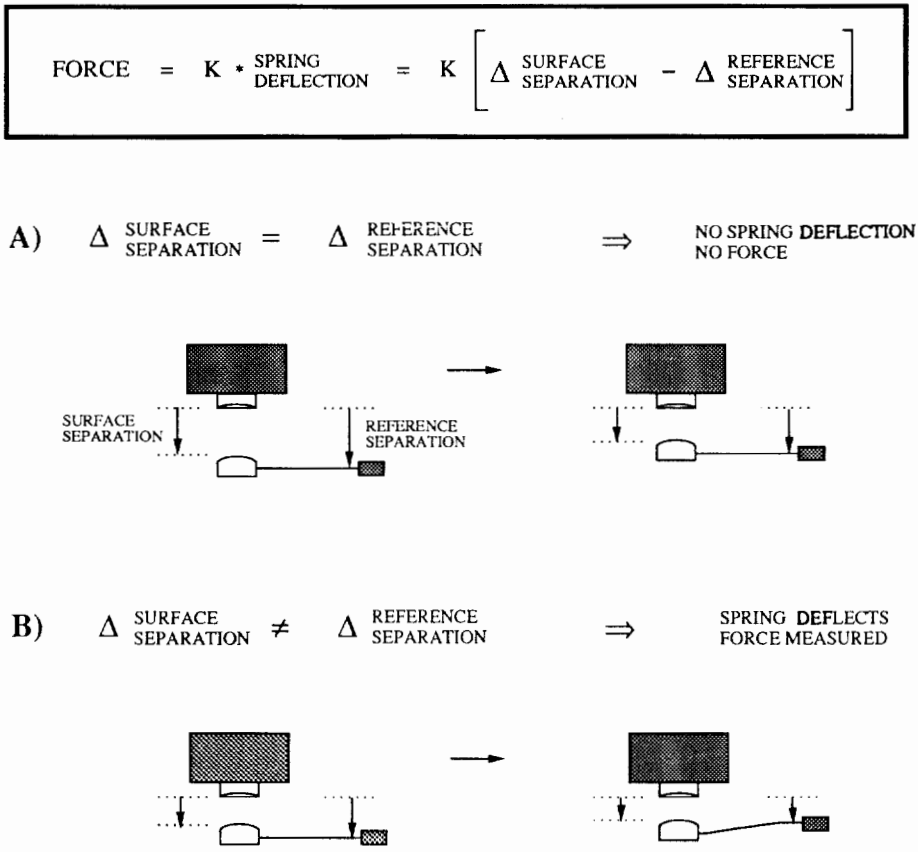

Fig. 2. Method of force measurement. Mechanisms used to change the reference separation are calibrated at large surface separation, where no forces are present.

in force at two surface separations, D and D^*, is given by the spring constant, K, times the difference in spring deflection:

$$F-F^*=K\left[(D-D^*)-\frac{dD}{d\alpha}(\alpha-\alpha^*)\right] \tag{1}$$

Typically, the force at any distance D is determined relative to zero force (zero spring deflection) at some large distance D^*.

In the experiment, the surfaces are curved and the surface separation, D, refers to the shortest distance between the mica surfaces. If the range of the forces is small in comparison with the radii of curvature of the surfaces, then the Derjaguin approximation can be used to relate the forces exerted between curved surfaces to the energy between flat surfaces. According to this approx-

imation, the force exerted between crossed cylinders of radius R_1 and R_2 is related to the energy per unit, E, area between planes separated a distance D by

$$F(D)=2\pi\sqrt{R_1R_2}E(D) \tag{2}$$

where D is taken to be the shortest distance between the two cylinders. While the curvature of the cylindrical quartz lenses is fixed ($\approx$1–2 cm), the curvature of each mica sheet is determined by the curvature of the glue layer between the mica and the lens. The Derjaguin approximation is used to eliminate the dependence of the measured forces on the local radii of curvature of the mica surfaces, which can vary from one experiment to the next. The derivative of $E(D)$ with respect to D is the disjoining or solvation pressure between flat plates separated by the distance D.

One limitation inherent to the method of force measurement is that the force can only be measured at surface separations where the gradient of the force, $\mathrm{d}F/\mathrm{d}D$, is less than the spring constant K; at distances where the gradient of the force is greater than the spring constant, the leaf spring which supports the lower surface is mechanically unstable. At a limit of mechanical instability, where $\mathrm{d}F/\mathrm{d}D=K$, the surfaces jump spontaneously to a new separation, the reference separation being fixed. On a plot of force versus separation, the trajectory of this jump follows a line of slope equal to the spring constant, from the point of instability to the next stable intersection of the force curve [26,27]. Therefore, forces can be continuously measured up to a limit of stability, at which point the force changes discontinuously by an amount equal to the spring constant times the distance of the jump.

Mechanical points of instability play a crucial role in the measurement of forces which oscillate with separation. Consider a force curve which oscillates between attractive (negative) and repulsive (positive) forces with increasing amplitude as the separation decreases. Then, starting at large separation and continuously decreasing the reference separation, forces are measured up a series of discretely spaced repulsive walls; the surfaces jump from one wall to the next at points of instability located just past each force maximum. Because the distance, and therefore the jump, between the repulsive walls is small, it is difficult to determine accurately both the force and the separation at the points of instability located near each repulsive maximum.

On the other hand, starting at small separation and continuously increasing the reference separation, forces are measured until the separation increases to just past that at the nearest force minimum. Here, the surfaces jump apart to large separation, generally in the force-free regime. Such points of instability are termed "adhesive minima" because the surfaces seem stuck together as they are pulled apart.

In practice, the gradient of the force changes very rapidly in the vicinity of force maxima and minima, and so the points of mechanical instability nearly

coincide with the maxima and minima of the force curve. An important point is that the forces between an instability located near a force minimum and an instability located near the next force maximum at larger separation are experimentally inaccessible.

In addition to this inherent limitation, there is a practical limit on the magnitude of repulsive forces that can be measured with a spring of given stiffness. As the spring supporting the lower surface deflects, there is necessarily a lateral displacement of the lower surface relative to the upper. Excessive shearing of the mica surfaces associated with large compressive loads can cause local surface damage. This limitation can be circumvented by using a variable stiffness spring [6]; however, springs of fixed stiffness ($\approx 1 \cdot 10^3$ dyn cm^{-1}) were used in the experiments reported herein.

Certain features of the experimental technique allow adhesive force minima to be measured more precisely and accurately than repulsive force maxima; these are discussed in what follows.

If the external force required to overcome a repulsive force barrier exceeds a threshold, the glue between the mica and the quartz lens deforms, causing the surfaces to flatten about the point of contact. The force threshold depends primarily on the type of glue (ca $2 \cdot 10^3$ μN m^{-1} for epoxy resins) but also on the steepness of the force barrier [28] and the rate of approach [6]. Such surface deformations are readily observed by the interferometric technique. When the surfaces are deformed, the measured deflection of the leaf spring is greater than the disjoining force by an amount equal to the force required to deform the glue. The deformation of the glue is usually elastic; thus, as the external load is released, the glue layer returns to its original shape. Hence, the accuracy of the force measured at an adhesive minimum is not affected by such surface deformations.

Christenson and coworkers [6] have noticed in recent measurements of the solvation force in liquid alkanes between mica surfaces that the forces at the repulsive maxima are not as reproducibly measured as those at the adhesive minima. They suggested that the repulsive forces measured on approach depend on the rate at which the surfaces are brought together, and that this accounts for the variability of the force maxima measured within an experiment.

2.2. Experimental method

The surface forces apparatus was used to measure the solvation forces on mica surfaces immersed in OMCTS, cyclohexane and mixtures of the two liquids. Measurements of the solvation force in pure liquids between mica were carried out with the entire chamber of the apparatus ($V \approx 350$ cm^3) filled with the solvent.

Two different types of experiments were conducted to measure the solvation force in binary solutions. In the first type of experiment, designed to investi-

gate small changes in concentration, the chamber of the apparatus was filled with OMCTS and the concentration of cyclohexane was varied by injecting known amounts into the chamber. A magnetic stir bar placed in the bottom of the chamber was used to mix the liquids. As shown in Fig. 1, the chamber must be filled to near capacity to completely immerse the two mica surfaces; hence it is not possible to inject large amounts of additional liquid. For this reason, a second type of experiment was designed to investigate large changes in concentration. Solvation forces were first measured between mica surfaces separated by a drop ($V \approx 0.05$ cm^3) of OMCTS, and then the chamber was filled with a premixed solution of known concentration for subsequent measurement.

Ruby muscovite mica, obtained from the United Mineral and Chemical Company, New York, NY, was used in all experiments. The OMCTS was purchased from Fluka, Ronkonkoma, NY. Anhydrous "Gold-label" cyclohexane was purchased from Aldrich, Milwaukee, WI.

Solvents were prepared specifically to eliminate two key contaminants: particulates, which can lodge between the mica surfaces, and residual water dissolved in the solvents, which can dramatically affect the magnitudes of the measured forces. The OMCTS was purified by double vacuum distillation, at approximately 70°C, under a nitrogen atmosphere. The anhydrous cyclohexane was used without further purification. All solvents were passed through a Teflon filter (Nuclepore, Pleasanton, CA) upon injection into the surface forces apparatus.

2.3. Solvation forces measured in pure OMCTS and pure cyclohexane

Since the original experiment by Horn and Israelachvili [3], OMCTS has played the role of a reference liquid, having been repeatedly used in a host of experiments designed to determine the effects of temperature [29], water saturation [17], and surface roughness [30] on the solvation force. It has also been used in dynamical experiments designed to measure the effective viscosity of confined thin films [31,32].

Although it has not been emphasized in the literature, there is a variability of the measured solvation force, not explainable as measurement uncertainty, from one experiment to the next, as different mica surfaces are employed. Much of this irreproducibility has been ascribed to variations in residual water saturation [4,17]. Yet, solvation forces measured in OMCTS dried identically in situ over phosphorous pentoxide are not reproducible to within experimental error (cf. Refs [17] and [30]). This variability may be attributed to the exact chemical composition of the mica surfaces, their relative crystallographic orientation, or the effects of substances, such as water, that are physisorbed onto the mica surfaces as they are cleaved.

We measured the solvation force on mica sheets immersed in OMCTS in six separate experiments, using new mica surfaces in each. In no case did we mea-

sure the solvation force down to zero film thickness. As described in Section 2.1, there is a practical limit to the magnitude of repulsive forces that can be measured with a spring of fixed stiffness.

In each experiment, a statistical analysis of variance was used to assign the measurements of the adhesive minima to sample populations, each corresponding to a specific minimum. The analysis is based on a separation of the variance of all observations into two parts, one which measures the variations from one population to the next and one which measures the internal variations within each population. The individual measurements are assigned to specific sample populations are assigned by maximizing the level of confidence associated with the hypothesis that measurements are drawn from a set of statistically different populations. In each experiment, this level of confidence was greater than 99.99%.

Averaged over the six separate experiments, the period of the force oscillations, as determined from the relative distance between the sample means, is 7.7 ± 1.5 Å. This is slightly smaller than the molecular diameter of OMCTS: 9.2 Å as estimated from diffusion measurements [33]. The magnitudes of the forces at the minima decay exponentially with distance, i.e., $F_{\min} \propto \exp(-D/\lambda)$, where $F_{\min}$ is the magnitude of the attractive force at the adhesive minimum, D is the surface separation (at the point of closest approach), and λ is a characteristic decay length. The average decay length, over the set of six experiments, is 13.4 ± 1.3 Å. Although there was some variability in the measured solvation force over the set of six experiments, the mean period and decay length are the same to within ± 2 Å.

Measurements by Christenson and Blom [17] of the solvation force in OMCTS determine the mean period of the oscillations to be 8.5 ± 0.5 Å. This is smaller than the period determined in earlier experiments (≈ 10 Å) by Horn and Israelachvili [4], the difference being attributed to a lower residual water saturation. It is, however, slightly larger than the period reported here. They noted that the peak-to-peak amplitude of the solvation force, as determined by the difference between the force at a minimum and that at the adjacent maximum at a larger separation, decays exponentially with distance with a decay length approximately equal to 12 Å.

We measured the solvation force on mica sheets immersed in cyclohexane in three separate experiments. The mean period and decay length, averaged over the set of experiments, are 5.4 ± 1.5 and 10.3 ± 1.0 Å, respectively. Our results are similar to those of Christenson [5], who found a mean period of 5.6 Å. The molecular diameter of cyclohexane as determined from diffusion data is approximately 5.6 Å [34]. As with OMCTS, the measured solvation force varied as the mica surfaces were changed, although the mean period and exponential decay length remain statistically the same to within ± 2 Å.

2.4. Solvation forces in binary solutions of OMCTS and cyclohexane

Experiments designed to measure the concentration dependence of the solvation forces on mica surfaces immersed in binary solutions must be carefully controlled to eliminate variability attributed to other independent variables. One source of variability is the residual water saturation in the liquids [17]. Another source is the mica; forces measured between different pairs of mica surfaces in the same solvent, prepared in the same way, differ by more than the measurement uncertainty. Only recently have researchers begun to address the importance of the properties of the solid in determining the induced fluid microstructure and related macroscopic properties [35]. Thus, a systematic study of the solvation forces on mica surfaces in binary solution requires using the same mica substrates as the solvent composition is varied, and keeping the water saturation constant, and as low as possible.

The variation with separation of the force required to confine each pure liquid between mica sheets can be characterized in terms of the mean period and exponential decay length, both obtained from measurements of the adhesive force minima. We applied the analysis of variance to the results for pure OMCTS and cyclohexane. The mean periods of the solvation force in each liquid are statistically different to 99% confidence; the average decay lengths are statistically different to 98% confidence. Thus, as one liquid is added to the other, one effect that can be measured is the change in mean period and decay length.

In the first set of experiments, solvation forces were measured in binary solutions of OMCTS and cyclohexane as the bulk liquid concentration of cyclohexane was changed from 0 to 14 mol%. As the concentration of cyclohexane is increased from zero, the amplitude of the force curve decreases, i.e., the magnitudes of both the attractive and repulsive forces are diminished. As this happens, the minima at largest separation becomes too small to measure. Subsequently, the force maxima at smaller separations decrease and can be surmounted; the force minima at smaller separations can then be measured. The forces and locations of the measured adhesive minima at five different bulk concentrations are plotted in Fig. 3. As the concentration of cyclohexane is increased, the adhesive minima follow trajectories of decreasing force and smaller separation, i.e., closer distance relative to mica–mica contact (as measured in air). Although the locations and magnitudes of the force minima vary systematically with the addition of cyclohexane to OMCTS, the mean period and decay length in the concentration range studied, down to 86 mol% OMCTS, are not statistically different from those in pure OMCTS.

We performed two experiments designed to probe larger changes in concentration. In one case the concentration of cyclohexane was increased from 0 to 32 mol%. The mean period of the oscillations changed from 7.7 ± 1.3 Å in pure OMCTS to 6.7 ± 0.7 Å in the mixture. The decay length decreased from 13.7 to

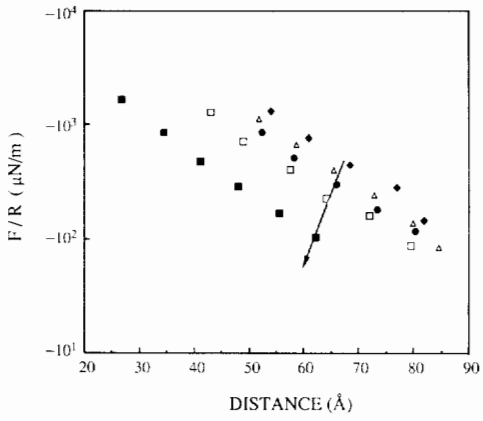

Fig. 3. Behavior of measured adhesive minima as cyclohexane is added to OMCTS: $x_1^b = 0.0$ (♦); 0.02 (△); 0.04 (●); 0.05 (□); 0.14 (■).

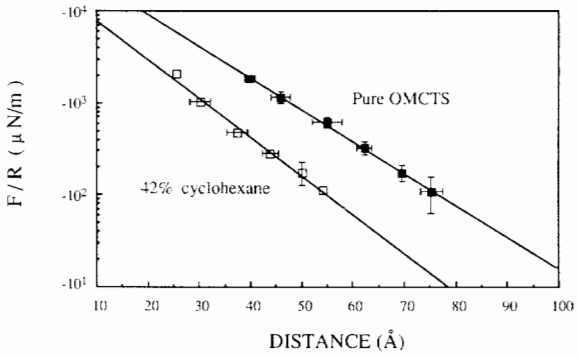

Fig. 4. Adhesive minima in a 42 mol% cyclohexane/OMCTS solution compared to those measured in pure OMCTS. The magnitudes of the forces at the adhesive minima follow an exponential decay: $F_{min} \propto e^{-D/\lambda}$.

11.2 Å. In the other experiment, the concentration of cyclohexane was increased from 0 to 42 mol%. As shown in Fig. 4, the mean period changed from 7.1 ± 1.2 Å in pure OMCTS to 5.8 ± 1.3 Å in the mixture; the decay length decreased from 12.6 to 10.2 Å.

The results of this study can be compared with the brief study by Christenson [19] of the same binary liquid system. He too found that as the mole percent of cyclohexane was changed from 0 to 10%, the amplitude of the forces decreased, whereas the period remained the same to within experimental uncertainty. However, within this concentration range he did not observe a shift in the positions of the minima to slightly smaller separations. At equimolar concentration, the positions of the adhesive minima were different from those

measured in pure OMCTS and the period was stated to be intermediate to that of pure OMCTS and cyclohexane.

Our results can also be compared with those of Christenson and Blom [17], who measured the solvation forces in "wet" OMCTS between mica surfaces; they equilibrated a drop of OMCTS between the mica surfaces with a vapor of known water activity. They observed a smooth decrease in the amplitude of the oscillations as the water activity in the vapor was increased from zero, with no change in the mean period. At 50% water activity, the period of the oscillations, as determined from the minima at large separation, was intermediate between that of the two pure liquids, although the spacing between the minima was quite irregular.

3. STATISTICAL MECHANICS OF CONFINED HARD ROD MIXTURES

This section is divided into two parts. In Section 3.1 we present the governing equations for a multicomponent hard rod fluid confined on a line of finite length. In Section 3.2, we use the results to predict the density profiles, average concentration, and disjoining pressure of the confined fluid.

3.1. Governing equations

We consider the equilibrium properties of a hard rod fluid confined on a line of length L. No external potentials act on the fluid other than that which defines the length of the line segment. The external potential acting on a particle of component i with diameter d_i is given by

$$\begin{aligned} u_i^{\text{ext}}(x) &= 0, \quad \frac{d_i}{2} \le x \le L - \frac{d_i}{2} \\ &= \infty \quad x < \frac{d_i}{2},\ x > L - \frac{d_i}{2} \end{aligned} \tag{3}$$

Thus the center of a particle with diameter d_i is strictly prohibited from lying within $d_i/2$ of each end of the line segment.

The canonical partition function is analytically solvable and provides exact expressions for all thermodynamic properties of the inhomogeneous fluid. For a c-component system, containing N_i particles of component i such that $\sum_{i=1}^{c} N_i = N$, the result is

$$Q_{\mathbf{N}} = \left(\prod_{i=1}^{c} \frac{1}{N_i! \Lambda_i^{N_i}} \right) \eta \left(L - \sum_{j=1}^{c} N_j d_j \right) \left(L - \sum_{j=1}^{c} N_j d_j \right)^{N} \tag{4}$$

Here η is the Heaviside step function and Λ_i is the de Broglie thermal wavelength of component i, given by

$$\Lambda_i = \left(\frac{h^2}{2\pi m_i kT} \right)^{1/2} \tag{5}$$

where h is Planck's constant, k is Boltzmann's constant, m_i is the particle mass of component i, and T is the temperature. Note that $Q_{\mathbf{N}} = 0$ when the total excluded volume of the particles, given by $\sum_{j=1}^{c} N_j d_j$, is greater than L.

The equilibrium properties of an open isothermal system of hard rods on a line of length L follow directly from the grand partition function, Ξ_L, which can be expressed as a weighted sum of canonical partition functions:

$$\Xi_L = \sum_{N_1=0}^{\infty} \cdots \sum_{N_c=0}^{\infty} \lambda_1^{N_1} \cdots \lambda_c^{N_c} Q_{\mathbf{N}} \tag{6}$$

Here λ_i is the activity of component i, defined by

$$\lambda_i \equiv e^{\mu_i / kT} \tag{7}$$

where μ_i is the chemical potential of component i.

All thermodynamic properties of the open system follow from the grand partition function. In particular, the pressure is given by

$$P = kT \left(\frac{\partial \ln \Xi_L}{\partial L} \right)_{T, \mu_1, \ldots, \mu_c} \tag{8}$$

The average number of particles of component i, $\bar{N}_i$, is given by

$$\bar{N}_i = kT \left(\frac{\partial \ln \Xi_L}{\partial \lambda_i} \right)_{T, \mu_1, \ldots, \mu_{i-1}, \mu_{i+1}, \ldots \mu_c} \tag{9}$$

Alternatively, the equilibrium value of any property X in the open isothermal system can be expressed as the grand canonical ensemble average of $X_{\mathbf{N}}$, given by

$$\langle X \rangle_{GC} = \sum_{N_1=0}^{\infty} \cdots \sum_{N_c=0}^{\infty} X_{\mathbf{N}} \mathscr{P}_{\mathbf{N}} \tag{10}$$

where $X_{\mathbf{N}}$ is the corresponding property for a closed isothermal system composed of N_i particles of component i, and $\mathscr{P}_{\mathbf{N}}$ is the probability of observing such a system in the grand canonical ensemble. The probability $\mathscr{P}_{\mathbf{N}}$ is given by

$$\mathscr{P}_N = \frac{\left(\frac{\lambda_1^{N_1}}{N_1!\Lambda_1^{N_1}}\right)\cdots\left(\frac{\lambda_c^{N_c}}{N_c!\Lambda_c^{N_c}}\right)\eta\left(L-\sum_{j=1}^{c}N_j d_j\right)\left(L-\sum_{j=1}^{c}N_j d_j\right)^N}{\Xi_L} \tag{11}$$

The kth body density distribution function, n^k, is defined such that $n^k(x_1, \cdots, x_k; L)\mathrm{d}x_1, \cdots, \mathrm{d}x_k$ represents the probability of finding the center of a particle within $x_1+\mathrm{d}x_1$, the center of a particle within $x_2+\mathrm{d}x_2$, etc., up to k particles. For a single-component hard rod fluid confined on a line of finite length, Robledo and Rowlinson [36] have shown that the kth body density distribution function is given by

$$n^k(x_1,\cdots,x_k;L) = \frac{\zeta^k \Xi_{x_1-d/2}\left(\prod_{l=2}^{k}\Xi_{x_l-x_{l-1}-d}\right)\Xi_{L-x_k-d/2}}{\Xi_L} \tag{12}$$

Here ζ is the reduced activity, defined by

$$\zeta \equiv \frac{\mathrm{e}^{\mu/kT}}{\Lambda} \tag{13}$$

and Ξ_x is the grand partition function for an open system characterized by length x and reduced activity ζ. For values of x less than zero, $\Xi_x \equiv 0$. For x equal to zero, $\Xi_x \equiv 1$.

Equation (12) follows from the fact that particles located at k positions, x_1, $\cdots$, x_k, serve to subdivide the original system of length L into $k+1$ systems of length $(x_1-\frac{d}{2})$, $(x_2-x_1-\mathrm{d})$, $\cdots$, $(x_k-x_{k-1}-d)$, and $(L-x_k-\frac{d}{2})$. For $k=1$, the singlet distribution function, which is the density, is given by

$$n(x) = \frac{\zeta \Xi_{x-d/2}\Xi_{L-x-d/2}}{\Xi_L} \tag{14}$$

which can be readily evaluated for all finite values of L.

The extension of this result to an open c-component system of hard rods confined on a line of length L follows directly. The kth body density distribution function is given by

$$n^k(x_1,\cdots,x_k;L) = \frac{\zeta_1\cdots\zeta_k \Xi_{x_1-d_1/2}\left(\prod_{l=2}^{k}\Xi_{x_l-x_{l-1}-(d_l+d_{l-1})/2}\right)\Xi_{L-x_k-d_k/2}}{\Xi_L} \tag{15}$$

where a particle at x_i has a diameter d_i. The reduced activity of component i is defined by

$$\zeta_i \equiv \frac{e^{\mu_i/kT}}{\Lambda_i} \tag{16}$$

The density of each component is then given by

$$n_i(x) = \frac{\zeta_i \Xi_{x-d_i/2} \Xi_{L-x-d_i/2}}{\Xi_L} \quad i=1,\cdots,c \tag{17}$$

3.2. Application to binary hard rod fluid confined in a slit-pore

We now use the exact theory of multicomponent hard rod fluid to investigate the behavior of a binary hard rod fluid on a line of finite length, i.e., the fluid is confined in a slit-pore. The pore fluid is in equilibrium with bulk fluid at fixed temperature, pressure and concentration.

The chemical potential of each fluid component is, of course, equal to the chemical potential in the bulk fluid. The thermodynamic properties of the bulk homogeneous fluid can be calculated from a canonical ensemble of systems as the length L goes to infinity at fixed density, N/L. In this case, the chemical potential of component i in bulk fluid at temperature T and pressure P is given by

$$\mu_i = kT \ln(\Lambda_i x_i^b P) + d_i P \tag{18}$$

where x_i^b is the mole fraction of component i in the bulk fluid.

We consider a binary hard rod fluid with $d_2 = 1.5d_1$. This relative size ratio is approximately that of OMCTS and cyclohexane. Density profiles of confined fluid in equilibrium with bulk fluid at a pressure of $3kTd_1^{-1}$ are shown in Fig. 5. The pore width varies from $2.0d_1$ to $3.5d_1$. Three separate bulk concentrations are examined: $x_1^b = 0.8$, 0.5 and 0.2. The density, $n_i(x)$, can be interpreted as the unnormalized probability of finding the center of a particle of component i at position x. The center of the slit-pore corresponds to $x=0$ (note, however, that the equations presented in Section 3.1 correspond to a slit-pore with the center at $x=L/2$).

At a given pore width, $\mathscr{P}_{N_1, N_2}$ is the probability that a pore is in an occupancy state corresponding to N_1 particles of component one and N_2 particles of component two, denoted hereafter by (N_1, N_2). The probability of a particular occupancy state depends on the chemical potentials of each component and is given by Eqn (11). Recall that a given occupancy state becomes permissible, i.e., occurs with non-zero probability, only if the length of the pore is greater than the excluded volume, $N_1d_1 + N_2d_2$. We now interpret the resulting density profiles in terms of permissible occupancy states.

At $L=2d_1$, for example, the permissible occupancy states are $(N_1,N_2) = \{(0,0),(1,0),(0,1)\}$. Note that the density distribution of each component is characteristic of a pore occupied by a single particle: the density is

uniform in the region of pore space where the external potential acting on that particular component is zero. As x_1^b decreases, $n_2(x)$, or equivalently the probability of finding the center of a particle of component two at x, increases while $n_1(x)$ decreases.

At $L=2.5d_1$, a new possibility is added to the set of permissible occupancy states: two particles of component one, $(N_1, N_2)=(2,0)$. The density profile of component one is thus a weighted superposition of two profiles: one characteristic of a pore occupied by a single particle and one characteristic of a pore occupied by two particles. For $(N_1, N_2)=(1,0)$, there is a finite probability that the center of the particle will be found in the center of the pore, i.e., $n_1(0)$ is non-zero. On the other hand, for $(N_1, N_2)=(2,0)$, $n_1(0)=0$.

At $L=3d_1$, another new possibility is added to the set of permissible occupancy states: $(N_1, N_2)=(1,1)$. At this larger pore width, the probability of $(N_1, N_2)=(1,0)$ is negligible, and so the density distribution of component one is now primarily determined from a weighted superposition of only two profiles: those corresponding to $(N_1, N_2)=(2,0)$ and $(N_1, N_2)=(1,1)$. One can easily identify the contributions from each profile to the resultant density profile of component one. For $(N_1, N_2)=(2,0)$, the density within the pore is zero only at $x=0$. For $(N_1, N_2)=(1,1)$, the density is identically zero in a finite region about the center: $n_1(x)=0$ for $|x|\leq 0.25$. The density distribution of component two is also a weighted superposition of two profiles, one corresponding to $(N_1, N_2)=(0,1)$ and one corresponding to $(N_1,N_2)=(1,1)$. In the first case, $n_2(0)$ is non-zero; in the second case, $n_2(0)=0$.

The results can be summarized as follows. At pore widths greater than d_1+d_2, two types of occupancy states can occur with non-zero probability: pure occupancy states composed of one or more particles of a single-component, or mixed occupancy states composed of one or more particles of both components. The probabilities of all pure occupancy states of component one fall continuously as x_1^b decreases, while the probabilities of all pure occupancy states of component two continuously rise. All mixed occupancy states occur, of course, with zero probability in the limits of $x_1^b=0$ and $x_1^b=1$. The probability of a permissible mixed occupancy state is a maximum at some intermediate bulk concentration, which depends on the length, relative sizes and chemical potentials of the fluid components.

As the bulk mole fraction approaches the limiting values of zero or one, the ensemble average properties of the confined binary fluid are dominated by pure occupancy states of the component which is in excess in the bulk fluid. At intermediate concentrations, however, the properties of the confined fluid are determined by both the permissible pure occupancy states and the numerous mixed occupancy states which can occur. The latter can, in many cases, completely dominate the ensemble average properties of the confined fluid. For

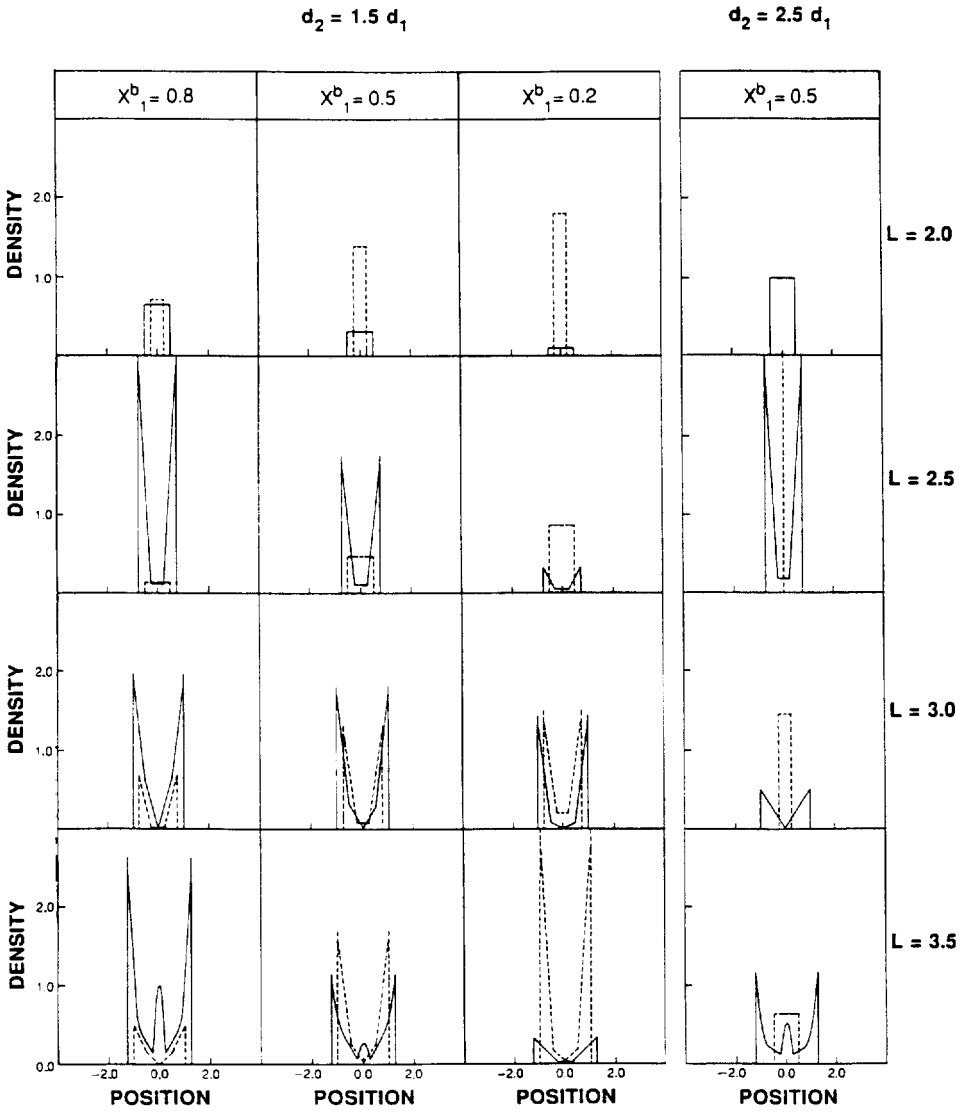

Fig. 5. Density profiles of a binary hard rod fluid confined in a one-dimensional slit-pore. The solid curves are the density profiles for component 1. The dashed curves are the density profiles for component 2: $d_2 = 1.5d_1$. The confined fluid is in equilibrium with bulk fluid at $P^b = 3kT/d_1$.

example at $L = 3.5d_1$, the (1,1) mixture occupancy state plays the dominant role in establishing the ensemble average properties at all three bulk compositions examined.

Density profiles of a binary hard rod fluid with $d_2 = 2.5d_1$ are also presented in Fig. 5. The behavior of this system is qualitatively similar to the binary fluid

with $d_2 = 1.5d_1$, and can be analyzed in terms of occupancy states as described above. Hence, density profiles are only shown for $x_1^b = 0.5$.

The average occupation number of particles of component i in the pore is given by

$$\bar{N}_i = \sum_{N_1=0}^{\infty} \cdots \sum_{N_c=0}^{\infty} N_i \mathscr{P}_{N_1,\ldots,N_c} \tag{19}$$

The total average occupation number, $\bar{N}$, is simply

$$\bar{N} = \sum_{i=1}^{c} \bar{N}_i \tag{20}$$

Unlike the total average occupation number, the average occupation number of each component does not necessarily increase monotonically with pore width. At a given pore width, the pore average mole fraction of component i, defined by

$$\bar{x}_i \equiv \bar{N}_i / \bar{N} \tag{21}$$

can be significantly different from the mole fraction of component i in the bulk fluid. There is a partitioning of fluid components between the confined and bulk fluids that is based on size selectivity. Figure 6 shows the variation with pore width of the pore average mole fraction at five different bulk concentrations. The pore average mole fraction of component one oscillates with pore width with a period that decreases as the mole fraction of component one in

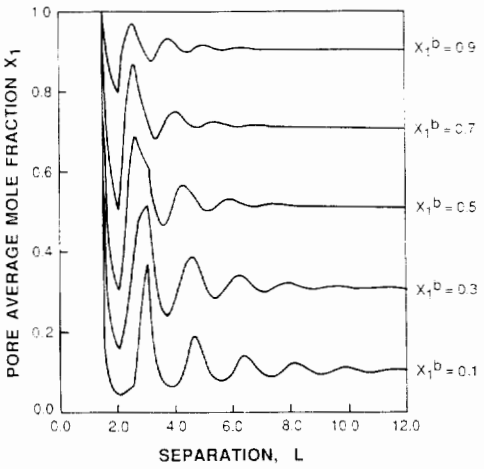

Fig. 6. Variation of pore average mole fraction with pore width in a binary hard rod fluid with $d_2 = 1.5d_1$. The bulk pressure is $P^b = 3kT/d_1$.

the bulk decreases. The selectivity of the pore increases with decreasing pore width.

The pressure of multicomponent fluid at a given pore width is given by the grand canonical ensemble average:

$$P(L)=\sum_{N_1}\sum_{N_2} P_{N_1,N_2}\mathscr{P}_{N_1,N_2} \qquad (22)$$
$$=\sum_{N_1}\sum_{N_2}\frac{kT(N_1+N_2)}{L-N_1d_1-N_2d_2}\mathscr{P}_{N_1,N_2}$$

The disjoining pressure, π, is defined as the difference between the normal stress in the pore fluid and the isotropic stress in the bulk fluid. In one dimension, the normal stress is equal to the pressure, as defined above; thus $\pi=P-P^{\text{bulk}}$. The solvation force between two flat solids immersed in a liquid is equal to the integral of the disjoining pressure over the area of interaction. The variation of disjoining pressure with pore width for a confined binary fluid with $d_2=1.5d_1$ is shown in Fig. 7 at five different bulk compositions, including the limiting cases of $x_1^b=0$ and $x_1^b=1$.

The pressure of the binary confined fluid can be decomposed into a sum of canonical weighted pressures, given by $P_{N_1,N_2}\mathscr{P}_{N_1,N_2}$. This product of the canonical pressure, P_{N_1,N_2}, times the probability of the given occupancy state, $\mathscr{P}_{N_1,N_2}$, is zero for pore widths less than the excluded volume, $N_1d_1+N_2d_2$, increases to a maximum at a pore width slightly larger than the excluded volume, and decreases monotonically to zero as the pore width goes to infinity. The probability of a given occupancy state, and hence the relative contribution of $P_{N_1,N_2}\mathscr{P}_{N_1,N_2}$ to the total pressure, is strongly dependent on the bulk fluid composition and pressure.

As the mole fraction of the second component in the bulk fluid is increased from zero, the variation with pore width of the ensemble average pressure reflects the following changes. First, there is a sharp increase in pressure at a pore length just past d_2. This is due to the fractional increase os states occupied by one particle of component two. As x_2^b continues to increase, similar increases in pressure commence at pore lengths just past each multiple of d_2. Not only does the resultant pressure curve reflect the increasing importance of occupancy states which consist only of particles of component two, it also reflects the relative decrease in probabilities of occupancy states which consist only of particles of component one. As x_2^b increases, one can observe the relative decrease in the pressure maxima associated with the canonical weighted pressure curves corresponding to pure occupancy states of component one.

Unlike the pure confined fluid, the variation with pore width of pressure in a binary fluid is complicated by the occurrence of mixed occupancy states. For example, one can see at intermediate concentrations sharp increases in pressure at pore widths just past d_1+d_2 and $2d_1+d_2$. The relative importance of the mixed occupancy states in determining the properties of the confined fluid

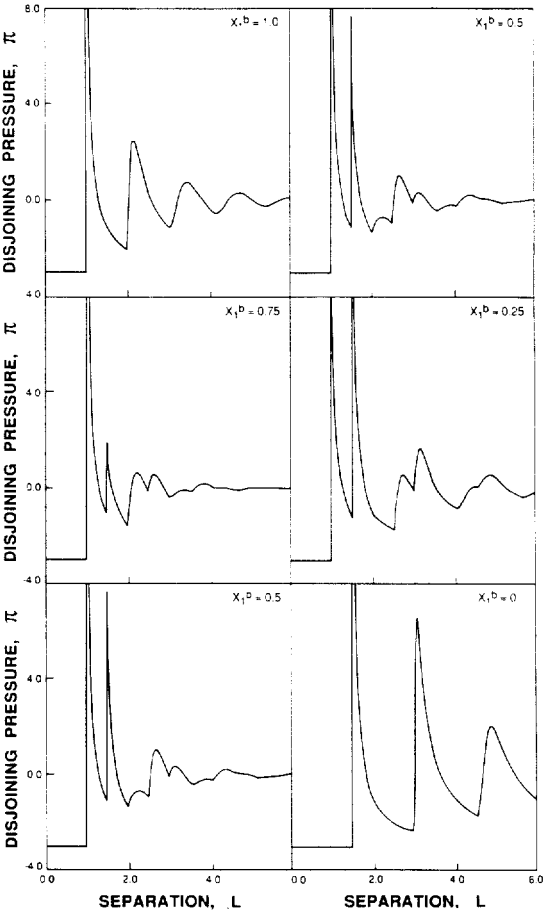

Fig. 7. Variation of disjoining pressure with pore width for a binary hard rod fluid with $d_2 = 1.5d_1$. The bulk pressure is $P^b = 3kT/d_1$.

is determined by the chemical potentials of the fluid components, their relative sizes, and the pressure of the bulk fluid.

4. COMPARISON OF THEORY AND EXPERIMENT

The theoretical analysis can be used to interpret measurements of the solvation force on mica surfaces immersed in mixtures of cyclohexane and OMCTS. Because the mica surfaces in the experiment are crossed cylinders, we measure $E(D) = \int_D^\infty \pi(D')dD'$ instead of $\pi(D)$. Qualitatively, however, $E(D)$ and $\pi(D)$ behave similarly with respect to the trends we wish to emphasize. Thus, we discuss the theoretical results in terms of $\pi(D)$.

First we compare the results for pure hard rod fluid confined between solid surfaces. Note from Fig. 7, that in the limit of single-component fluid, the disjoining pressure oscillates with increasing amplitude between positive and negative values, corresponding to repulsive and attractive solvation forces, as the separation decreases. In the limit of pure component 2 ($d_2 = 1.5d_1$), the average distance between successive minima is $1.1d_2$. Excluding the weakest minima at large separation, the magnitudes of the disjoining pressures at the local minima decay exponentially with separation. The characteristic decay length, based on the six minima at the smallest separations, is $2.5d_2$. The variation with pore width of the disjoining pressure in pure component one is qualitatively similar. The period of the oscillations as calculated from the mean distance between local minima is $1.2d_1$. The characteristic decay length is $1.5d_1$.

Experimentally, the solvation force is found to oscillate regularly between attraction and repulsion with a period equal to or slightly smaller than the diameter of the fluid molecules, as determined from the distance between successive adhesive minima. The magnitudes of the forces at the adhesive minima decay exponentially with separation with a characteristic decay length that is between 1.5 and 2 times the period of the oscillations. Clearly this behavior is qualitatively reproduced by the hard rod system. The mean periods predicted for the hard rod system are slightly larger in comparison, but the mean period is expected to decrease as the dimensionality of the system is increased from one to three.

We now compare the theoretical predictions with the experiments in binary solution. As shown in Fig. 7, the resulting changes in the variation with pore width of the disjoining pressure as the bulk fluid concentration is changed from pure 2 to pure 1 can be decomposed into three competing phenomena. First, as the bulk fluid concentration of 1 is increased from zero, the magnitudes of the disjoining pressure at the minima and maxima are diminished, and the locations of each maximum and minimum are slightly shifted. The minima and maxima originally present in the disjoining pressure curve of pure 2 are gradually washed out. The second phenomenon is the occurrence of a set of new local minima and maxima which appear as component 1 is added to component 2. These maxima and minima grow in continuously and become the corresponding minima and maxima in the disjoining pressure curve in pure 1. The third phenomenon is the occurrence of an additional set of minima and maxima which appear as component 1 is added to component 2. However, these minima and maxima eventually disappear as the concentration of the bulk fluid reaches pure 1.

Before the theoretical predictions can be compared with experimental measurements of the solvation force in mixtures, the role of mechanical instabilities in the force measurement technique, as described in Section 2.1, must be addressed. *Because of mechanical instabilities, not all theoretically predicted*

minima are experimentally accessible to the surface forces apparatus in its current design.

We thus assume that a predicted force minimum corresponds to an "experimentally accessible adhesive minimum" if the following conditions are true. First, the minimum must be experimentally accessible. Since each local minimum is located between two local maxima, this requires that the force at the local maximum at smaller separation be greater than the force at the local maximum at larger separation. Second, the minimum must be an adhesive minimum. This means that the surfaces must jump to large separation, in the force free regime, as they are pulled apart. This requires that the magnitude of the force at the minimum be larger than that at all local minima at larger separation. Third, the magnitude of the force at the minimum must be greater than the sensitivity of the apparatus used to measure the force.

Plotted in Fig. 8 are the experimentally accessible adhesive minima predicted for the hard rod system as the bulk fluid concentration of the smaller component, x_1^b, is increased from 0 to 14 mol%. As x_1^b is increased, the positions of the adhesive minimum shift to slightly smaller separation and their magnitudes fall. The mean period and decay length predicted at each bulk fluid concentration examined are reported in Table 1. In this concentration range, the mean period and exponential decay length remain similar to that in pure component 2.

Figure 9 shows the experimentally accessible adhesive minima predicted for an equimolar bulk fluid concentration; the results are compared to the limiting single-component results. In this case, the forces decay exponentially, although the decay length is smaller than that of either single-component fluid. The mean period is slightly smaller than the mean period predicted for pure component 1. At other intermediate concentrations, the mean period and decay length are generally intermediate between those predicted in either pure fluid.

The trends predicted theoretically are again consistent with those observed experimentally. As the concentration of the smaller component, cyclohexane, in the bulk liquid is increased from 0 to 14 mol%, the measured solvation forces remain oscillatory. However, the magnitudes of the adhesive minima decrease continuously and their locations shift slightly to smaller separations. The mean period and exponential decay of the forces at the adhesive minima remain the same as in pure OMCTS. At higher molar concentrations of cyclohexane, in particular 32 and 42%, the solvation force continues to alternate between attraction and repulsion, but the mean period and characteristic decay length are statistically different from those in pure OMCTS, and are intermediate to those in either cyclohexane or OMCTS.

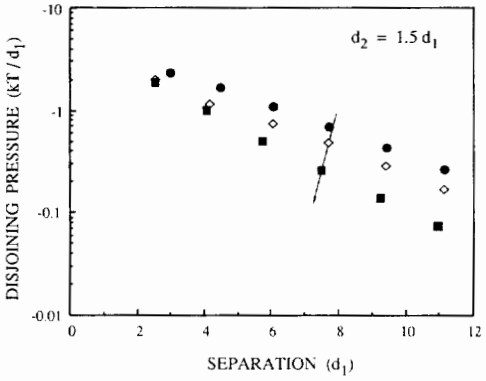

Fig. 8. Behavior of experimentally accessible adhesive minima for confined binary hard rod fluid, with $d_2 = 1.5d_1$, as component 1 is added to component 2: $x_1^b = 0$ (●); 0.05 (◇); 0.14 (■). The bulk pressure is $P^b = 3kT/d_1$.

TABLE 1

Mean period and exponential decay length of solvation forces in a binary hard rod fluid: $d_2 = 1.5d_1$. The confined binary fluid is in equilibrium with bulk fluid at $P^b = 3\,kTd_1$

x_1^b	Mean period (d_1)	Decay length (d_1)
0.00	1.64	3.70
0.05	1.60	3.58
0.14	1.69	2.62
0.50	1.61	1.29
1.00	1.17	1.53

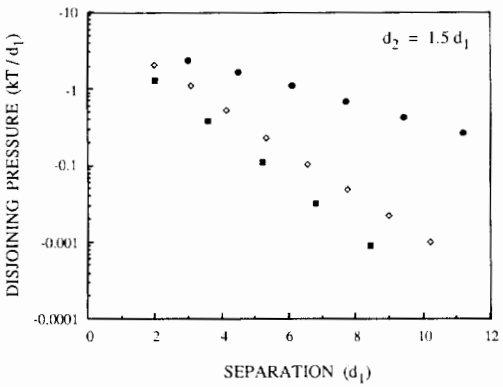

Fig. 9. Experimentally accessible adhesive minima for confined binary hard rod fluid, with $d_2 = 1.5d_1$, in equilibrium with bulk fluid at equimolar concentration. Results are compared with adhesive minima for confined single-component hard rod fluids: $x_1^b = 0$ (●); 0.50 (■); 1 (◇). The bulk pressure is $P^b = 3kT/d_1$.

Recently, Vanderlick et al. [37] have extended the generalized hard rod model for a three-dimensional fluid to multicomponent systems. This model reduces to the exact one-dimensional result for hard rods in an external field. Application of the model to three-dimensional binary fluid confined between solid surfaces will be reported in a future publication. We note here, however, that all the trends observed in the one-dimensional system are carried over to the three-dimensional system.

ACKNOWLEDGEMENTS

The authors are grateful to the ACS Petroleum Research Fund, the National Science Foundation, the Department of Energy, and the Minnesota Supercomputer Institute for financial support of this research.

REFERENCES

1 W. van Megen and I.K. Snook, J. Chem. Soc. Faraday Trans. 2, 75 (1979) 1095.
2 J.E. Lane and T.H. Spurling, Chem. Phys. Lett., 67 (1979) 107.
3 R.G. Horn and J.N. Israelachvili, Chem. Phys. Lett., 71 (1980) 1922.
4 R.G. Horn and J.N. Israelachvili, J. Chem. Phys., 75 (1981) 1400.
5 H.K. Christenson, J. Chem. Phys., 78 (1983) 6906.
6 H.K. Christenson, D.W.R. Gruen, R.G. Horn and J.N. Israelachvili, J. Chem. Phys., 87 (1987) 1834.
7 S. Nordholm, M. Johnson and B.C. Freasier, Aust. J. Chem., 33 (1980) 2139.
8 M. Johnson and S. Nordholm, J. Chem. Phys., 75 (1981) 1953.
9 P. Tarazona, Phys. Rev. A, 31 (1985) 2672.
10 T.F. Meister and D.M. Kroll, Phys. Rev. A, 31 (1985) 4055.
11 W.A. Curtin and N.W. Ashcroft, Phys. Rev. A, 32 (1985) 2909.
12 A. Robledo and C. Varea, J. Stat. Phys., 26 (1981) 513.
13 J. Fischer and U. Heinbuch, J. Chem. Phys., 31 (1988) 1909.
14 J. Fischer and M. Methfessel, Phys. Rev. A, 22 (1980) 2836.
15 T.K. Vanderlick, L.E. Scriven and H.T. Davis, J. Chem. Phys., 85 (1986) 6699.
16 T.K. Vanderlick, L.E. Scriven and H.T. Davis, J. Chem. Phys., 90 (1988) 2422.
17 H.K. Christenson and C.E. Blom, J. Chem. Phys., 86 (1987) 419.
18 H.K. Christenson, R.G. Horn and J.N. Israelachvili, J. Colloid Interface Sci., 88 (1982) 1834.
19 H.K. Christenson, Chem. Phys. Lett., 118 (1985) 455.
20 S. Nordholm, P. Harrowell and K. Cheung, Aust. J. Chem., 35 (1982) 247.
21 J. Fischer, personal communication.
22 J.L. Percus, J. Stat. Phys., 15 (1976) 505.
23 T.K. Vanderlick, H.T. Davis and J.K. Percus, J. Chem. Phys., 91 (1989) 7136.
24 D. Tabor and R.H.S. Winterton, Proc. R. Soc. A, 312 (1969) 435.
25 J.N. Israelachvili and G.E. Adams, J. Chem. Soc. Faraday Trans. 1, 74 (1978) 975.
26 K.B. Lodge and R. Mason, Proc. R. Soc. A, 383 (1982) 279.
27 K.B. Lodge and R. Mason, Proc. R. Soc. A, 383 (1982) 295.
28 B.D. Hughes, Ph.D. Thesis, Australian National University, 1980.
29 H.K. Christenson and J.N. Israelachvili, J. Chem. Phys., 80 (1984) 4566.
30 H.K. Christenson, J. Phys. Chem., 90 (1986) 4.

31 D.Y.C. Chan and R.G. Horn, J. Chem. Phys., 83 (1985) 5311.
32 J.N. Israelachvili, J. Colloid Interface Sci., 110 (1986) 263.
33 J.A. Barrie, R.B. Dawson and R.M. Sheppard, J. Chem. Soc., Faraday Trans. 1, 74 (1978) 490.
34 K.J. Czworniak, H.C. Anderson and R. Pecora, J. Chem. Phys., 11 (1975) 451.
35 P.M. McGuiggan and J.N. Israelachvili, Chem. Phys. Lett., 149 (1988) 469.
36 A. Robledo and J.S. Robinson, Molec. Phys., 58 (1986) 711.
37 T.K. Vanderlick, L.E. Scriven, J.K. Percus and H.T. Davis, in preparation.